

METHODOLOGY

Open Access



High precision measurement of trace F and Cl in olivine by electron probe microanalysis

Di Zhang^{1,2}, Yi Chen^{1,2*} , Bin Su¹, Chao Qi³ and Qian Mao¹

Abstract

Fluorine (F) and chlorine (Cl) are important volatiles in olivine and its high-pressure polymorphs, which would significantly affect olivine phase transition, melting temperature, and physical property of the mantle. F and Cl concentrations in olivine can be detected by electron probe microanalysis (EPMA). However, the analytical accuracy and precision can be impeded by severe peak overlaps, low peak intensities of traditional analytical crystals, and secondary fluorescence effects. In this study, we constructed an optimized analytical method with high accuracy and precision to analyze trace F and Cl in olivine. Key parameters of analytical crystals, beam conditions, peak overlaps, and secondary fluorescence effects were discussed. Variations in the levels of the analyzed trace elements fall within $\pm 10\%$. The detection limits (3σ) for F and Cl are lowered to 30 ppm and 5 ppm, respectively. This method can provide precise F and Cl analysis for natural olivine samples and help to provide significant information on its formation process.

Keywords Electron probe microanalysis, Olivine, Trace F and Cl, Secondary fluorescence effects

1 Introduction

Fluorine and chlorine are important volatiles concentrated in hydrous minerals and glasses via substitution with hydroxyl (Antignano 2008; Botcharnikov 2010; Bucher and Stober 2010; Li et al. 2022). F and Cl can significantly influence the physicochemical properties of melts/fluids and the geochemical behavior of trace elements (Keppler 1993; Filiberto and Treiman 2009; Bartels et al. 2011), so they play an important role in magmatic evolution, element cycling, and metal mineralization (Zhang et al. 2012; Kendrick et al. 2015; Kusebauch et al. 2015). In addition, some nominally anhydrous minerals, such as olivine, pyroxene, and garnet (Scambelluri et al. 2004; Beyer et al. 2012; Mosenfelder and Rossman 2013a,

b), could also have trace F and Cl. Olivine and its high-pressure polymorphs (wadsleyite and ringwoodite) are the principal rock-forming minerals in the upper mantle and mantle transition zone; they are also present in meteorites and lunar basalts (Chen 2005; Klemme and Stalder 2018; Tian et al. 2021). Dozens to hundreds ppm F and Cl could be detected in natural olivine samples, such as ~ 30 – 240 ppm F in olivine from mantle xenoliths (Hervig and Bell 2005) and ~ 10 – 120 ppm Cl in metamorphic olivine derived from serpentinites (Scambelluri et al. 2004; Debret et al. 2014). Olivine and its high-pressure polymorphs (wadsleyite and ringwoodite) in experimental products could contain considerable F and Cl over hundreds to thousands of ppm (e.g., Dalou et al. 2012; Bernini et al. 2013; Roberge et al. 2015, 2017; Grützner et al. 2018; Clarke et al. 2020; Potts et al. 2021).

F incorporation in olivine, wadsleyite, and ringwoodite may have the following mechanisms. F can replace oxygen in forsterite linked with a metal (Mg) vacancy for charge balance: $[\text{MgO}_2]^{2-} = [\square\text{F}_2]^{2-}$ (e.g., Beyer et al. 2012; Bernini et al. 2013). Crépisson et al. (2014) described a coupled incorporation of F and OH forming the $[\text{SiO}_{4-x-y}\text{F}_x(\text{OH})_y]^{4-}$ tetrahedrons in forsterite

*Correspondence:

Yi Chen
chenyi@mail.jggcas.ac.cn

¹ State Key Laboratory of Lithospheric Evolution, Institute of Geology and Geophysics, Chinese Academy of Sciences, Beijing 100029, China

² College of Earth and Planetary Sciences, University of Chinese Academy of Sciences, Beijing 100049, China

³ Key Laboratory of Earth and Planetary Physics, Institute of Geology and Geophysics, Chinese Academy of Sciences, Beijing 100029, China

(with $x+y \leq 4$), which was also confirmed by coupled OH–F-incorporation for wadsleyite and ringwoodite (Roberge et al. 2015). Grützner et al. (2018) proposed that the replacement of a $[\text{SiO}_4]^{4-}$ tetrahedron by a $[\text{F}]^{4-}$ quadruplet is the dominant mechanism for F incorporation in wadsleyite. An additional mechanism by which F is incorporated in olivine is forming a planar defect, where monolayers of a hydrous phase are formed (Wirth et al. 2001; Hermann et al. 2007). Cl, F, and OH may occupy similar sites in the olivine lattice, most likely associated with Mg vacancies (Roberge et al. 2017). F and Cl can significantly affect olivine phase transition, melting temperature, and element partition of the mantle (Roberge et al. 2015, 2017; Grützner et al. 2018).

Trace F and Cl in olivine were mostly detected in situ by secondary ion mass spectrometry (SIMS). Intensities of F and Cl in olivine show good linear relationships with those of Si during SIMS analysis (Beyer et al. 2012; Dalou et al. 2012; Potts et al. 2021). Therefore, homogeneous and well-certified calibration standards are necessary for F and Cl measurements. Glass standards, such as those from NIST and MPI-DING, were mostly used in previous studies (Dalou et al. 2012; Clarke et al. 2020; Potts et al. 2021). Only a few studies used F-implanted reference materials as calibration standards (Beyer et al. 2012; Bernini et al. 2013). However, F and Cl heterogeneity in some glass samples may lead to errors (Mosenfelder et al. 2011; Mosenfelder and Rossman 2013a, b). The surface and structure of F-implanted mineral standards could be severely altered during implantation, thus resulting in errors (Klemme and Stalder 2018). Besides, SIMS is destructive to precious samples, such as olivine in lunar meteorites. The large differences in olivine F and Cl contents reported may be caused by the different analytical methods of SIMS (Klemme and Stalder 2018). In addition, Crépeisson et al. (2014) and Roberge et al. (2017) used particle-induced X-ray/ γ -ray emission (PIXE or PIGE) to determine F and Cl content in olivine. These methods only obtained the averaged values of F and Cl contents in larger scanning regions (30×30 – $100 \times 150 \mu\text{m}^2$), which may lose detailed information on heterogeneous samples within micron scales.

In contrast to the techniques mentioned above, EPMA could provide advantages of high spatial resolution and nondestructive nature, making it valuable to develop a specific, high precision method to acquire low concentrations of F and Cl in olivine. Previous studies used EPMA to determine trace F and Cl in glass and hornblende (Vanko 1986; Donovan et al. 1993; Witter and Kuehner 2004; Zhang et al. 2016; Fletmetakis et al. 2020) and lowered the F detection limit to 82 ppm (3σ) and Cl detection limit to 28 ppm (3σ) (Zhang et al. 2016; Fletmetakis et al. 2020). However, these detection limits are much

higher than F and Cl concentrations in most natural olivine samples (e.g., Scambelluri et al. 2004; Hervig and Bell 2005; Beyer et al. 2012; Debret et al. 2014). Therefore, lower detection limits of F and Cl are strongly needed for olivine. Besides, secondary fluorescence effects from chlorine in epoxy resin could bring analytical errors to the points near the olivine boundary, which had never been discussed in previous studies and should not be neglected.

This study aims to develop a new method to improve precision, accuracy, and lower detection limits for trace F and Cl analysis in olivine. Optimal beam conditions, analytical crystals, and peak overlap are mainly discussed. Secondary fluorescence effects from epoxy resin on trace Cl analysis in olivine are also emphasized. In addition, the accuracy and precision of this method are evaluated based on the replicate analysis of hornblende reference materials with literature data. Our method can be successfully applied to natural olivine samples.

2 Samples

Basaltic glass is often used for trace F and Cl analysis by SIMS (e.g., Dalou et al. 2012; Clarke et al. 2020; Potts et al. 2021). However, glass is sensitive to beam current, leading to a higher EPMA detection limit when using low beam current and short analysis time. Hornblende is a silicate mineral containing hundreds to over thousands ppm of F and Cl, which can be used as secondary reference material for trace F and Cl analysis by EPMA (Zhang et al. 2016). Their F and Cl concentrations determined by Zhang et al. (2016) are as follows: 1673 ± 51 ppm F and 237 ± 10 ppm Cl for Kakanui hornblende, 361 ± 46 ppm F and 208 ± 17 ppm Cl for Arenal hornblende. Although Kakanui hornblende has some submicrometer-scale melt inclusions, which leads to slight major element variations, it could also be used as an internal secondary standard. Here, we used Kakanui hornblende (NMNH 143965) and Arenal hornblende (NMNH 111356) to evaluate the accuracy and precision of trace F and Cl analysis in olivine using EPMA.

Synthetic olivine samples were prepared using procedures similar to those described in (Zhao et al. 2009) and briefly summarized below. Fayalite, $\text{Fo}=0$, powders were synthesized in a one-atmosphere furnace from powders of Fe_2O_3 and SiO_2 in a molar ratio of 1:1.002 at 1353 K at controlled oxygen partial pressure. Powders of Fo_{70} , Fo_{50} , and Fo_{30} were then synthesized from a mixture of commercial forsterite, Fo_{100} , and this synthetic Fo_0 powder. For each composition, the mixed powders were ground to a particle size of $< 25 \mu\text{m}$ and reacted together at 85% of the solidus temperature in a one-atmosphere furnace for 20 h with oxygen fugacity buffered by a mixture of CO and CO_2 at an oxygen partial pressure equivalent to that

produced by a Ni/NiO solid-state buffer. After cooking, the powders were ground and reacted again to ensure the composition was uniform throughout the powders. Samples of Fo_{70} , Fo_{50} , Fo_{30} , and Fo_0 were then fabricated by first cold-pressing powders into nickel (Fo_{70} , Fo_{50} , and Fo_{30}) or iron (Fo_0) capsules and then hot-pressing the assemblies. Details of hot-pressing experiments can be found in Zhao et al. (2009). After hot-pressing, the densified iron-rich olivine samples were cut into thin slices for analysis. High-quality backscattered electron images show that the synthetic olivine samples are homogeneous at a scale of 30–50 μm , although there exist small amounts of tiny holes and residual glass (Additional file 1: Fig. S1). The homogeneous area is sufficient for EPMA measurement, and our results also indicate that these standards are compositional homogeneous (Additional file 2: Table S1).

Two natural olivine samples are selected to test the feasibility of this optimized method. Natural olivine samples (OL-1) are bought from a gem trader in Mogok, Myanmar. They are pale green, subhedral to euhedral crystals with grain sizes ranging from 0.2 to 1 cm. Olivine grains were first disaggregated into small blocks, handpicked under a binocular microscope, and mounted in epoxy resin for further analysis (Additional file 1: Fig. S2a and b). Natural olivine samples (OL-2) were collected from an olivine–antigorite serpentinite (sample J4) in the Hkamti Jade Mine Tract, Myanmar (Chen et al. 2018). Two generations of olivine can be observed in the serpentinite: primary mantle olivine cores and secondary Mg-rich olivine rims (Additional file 1: Fig. S2c and d). The primary olivine cores have a forearc mantle origin, whereas the secondary rims formed from antigorite dehydration at the slab–mantle interface (Chen et al. 2018).

3 Analytical method

All the experiments were conducted by CAMECA SXFive electron probe microanalyzer at IGGCAS. This instrument is equipped with five wavelength spectrometers and uses PeakSight software.

3.1 Analytical crystals

Analytical crystals diffract X-rays with specific wavelength λ following Bragg's law to the proportional counters. Two crystal geometries are generally used in EPMA: Johann and Johansson (Johann 1931; Johansson 1933). Adopting an appropriate analytical crystal would enhance X-ray intensities, reduce detection limits, and improve precision levels. Conventional TAP crystal and synthetic multilayered diffraction crystals (W/Si; termed LDE1 ($2d=60 \text{ \AA}$) by JEOL and PC0 ($2d=45 \text{ \AA}$) and PC1 ($2d=60 \text{ \AA}$) by CAMECA) can be used to analyze F. Due to the low count rates for F $K\alpha$ X-rays when using TAP

analytical crystals, low detection limit and high precision for trace F analysis could not be achieved (Potts and Trindle 1989). The synthetic multilayered diffraction crystals, customized for the diffraction of light element X-rays, provide much higher count rates and peak/background (P/B) ratios and are beneficial to trace F analysis though peaks are wide and attention paid to possible interferences (Witter and Kuehner 2004; Zhang et al. 2016; Flenetakis et al. 2020). For example, by measuring the F content of a CaF_2 sample using our CAMECA SXFive EPMA instrument, the F peak count rates are ca. 7 and 258 cps/nA (counts per second per nA) using TAP and PC1 crystals, respectively, showing a substantial improvement of the count rate by a factor of 37 when using the PC1 crystal. The P/B ratio of F $K\alpha$ X-ray using PC1 crystal was 54, which was triple higher than that of TAP (P/B=17). PC0 analyzing crystal could provide a higher count rate than TAP crystal and weaker peak interference than PC1 crystal. Therefore, if equipped in the probe, PC0 crystal would be a better choice for F analysis. Given the available analytical crystals and spectrometers in this instrument, the PC1 analytical crystal in spectrometer 1 was used to analyze trace F in olivine.

Two spectrometers in our electron microprobe analyzer are equipped with large-area Bragg crystals (LLIF, LPET). These large-area Bragg crystals provide higher intensities and P/B ratios than the normal area crystals, which can lead to lower detection limits and are more useful to trace element analyses. For example, the count rates for Cl were ca. 407 and 915 cps/nA using PET and LPET crystals, respectively, when acquiring the peak intensities of Cl $K\alpha$ X-rays of a NaCl sample using our CAMECA SXFive EPMA instrument. The P/B ratios for Cl $K\alpha$ X-rays were ca. 373 and 597 using PET and LPET crystals, respectively. With the software's aggregate intensity counting capacities, the X-ray intensities of different spectrometers can be added together, thus improving the counting rate and the analytical efficiency. Therefore, two LPET crystals in spectrometers 3 and 5 are used for trace Cl analysis in olivine.

3.2 Beam current

Some materials rich in F and Cl are sensitive to beam current, such as apatite and glass, leading to changes in X-ray counts over time or sample damage (e.g., Almasi et al. 1965; Borom and Hanneman 1967; Morgan and London 1996, 2005; McCubbin et al. 2011; Zhang et al. 2016). A low beam current of 10–20 nA was commonly used to acquire F and Cl, with detection limits over thousands of ppm (Stormer et al. 1993; McCubbin et al. 2011). Higher beam current could help to decrease F and Cl detection limit. Zhang et al. (2016) used 180 nA to lower the detection limit of F in hornblende to 82 ppm (3σ).

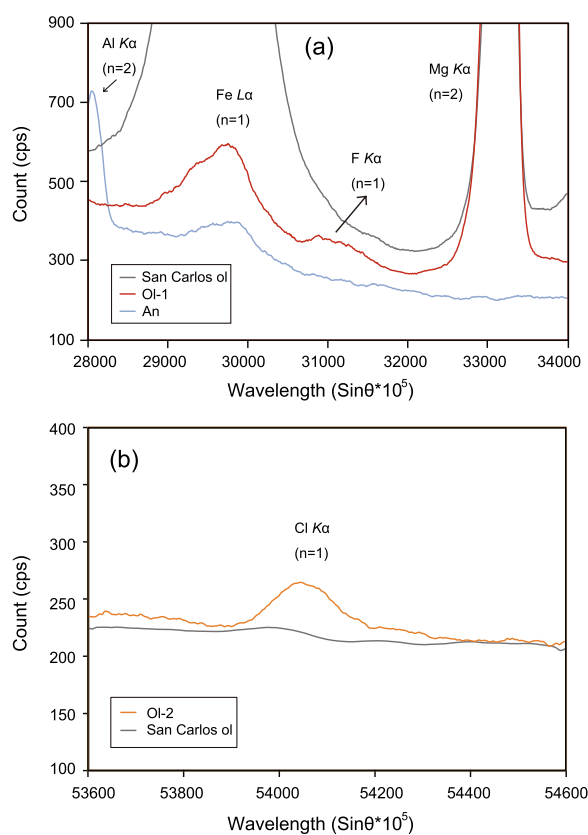


Fig. 1 **a** Smoothed averaged accumulated spectral scans of San Carlos olivine, natural olivine (Ol-1), and anorthite at the F $K\alpha$ peak acquired with PC1 diffraction crystal on CAMECA SXFive microprobe. Accelerating voltage = 20 kV; beam current = 200 nA; beam diameter = 10 μm ; dwell time = 500 ms; step = 10 ($\text{Sin}\theta \times 10^5$); accumulation number = 5; and differential mode: base line = 2300 mV, window = 2170 mV. **b** Smoothed averaged accumulated spectral scans of San Carlos olivine and natural olivine (Ol-2) at the Cl $K\alpha$ peak acquired with LPET diffraction crystal on CAMECA SXFive microprobe. Accelerating voltage = 20 kV; beam current = 400 nA; beam diameter = 5 μm ; dwell time = 500 ms; step = 5 ($\text{Sin}\theta \times 10^5$); accumulation number = 5; and integral mode. Mineral abbreviations are from Whitney and Evans (2010)

Flemetakis et al. (2020) utilized 60 nA to lower F and Cl detection limits for glass to 88 (3σ) ppm and 28 ppm (3σ), respectively. However, these detection limits are insufficient to obtain precise F and Cl concentrations in natural olivine (Hervig and Bell 2005; Beyer et al. 2012; Debret et al. 2014). High beam currents up to 900 nA were successfully used to lower the detection limits of Ca, Al, Ti, and other trace elements in olivine to below 10 ppm (Batanova et al. 2015; Su et al. 2019; Zhang et al. 2022a). Absorbed current and characteristic X-ray intensities of these elements keep steady under a 12 min electron beam bombardment (Batanova et al. 2015). Whether high beam current is suitable for trace F and Cl analysis in

olivine is still unknown. As shown in Fig. 1a, the natural olivine sample (Ol-1) shows a small F $K\alpha$ peak, whereas San Carlos olivine and anorthite show no peak at the F $K\alpha$ peak. The natural olivine sample Ol-2 exhibits a small Cl $K\alpha$ peak as well. In contrast, San Carlos olivine does not show an obvious Cl $K\alpha$ peak (Fig. 1b). Given that there is no available olivine standard for trace F and Cl analysis, we used the hornblende standards mentioned above as reference materials to evaluate the accuracy and precision. Therefore, we measure the X-ray intensities of F ($K\alpha$, PC1) and Cl ($K\alpha$, LPET) under various beam conditions at 20 kV for the natural olivine and Kakanui hornblende.

The Recorder utility in PeakSight software was used to record the changes in element signals in 10 min. Two beam conditions can be utilized in one analytical setting by this software. A lower beam current (30 nA with a beam diameter of 5 μm in this study) was used to analyze major elements, while a higher beam current can be used for minor/trace elements analysis.

As shown in Additional file 1: Fig. S3, the X-ray intensities of F, Cl, and the absorbed beam currents in natural olivine keep stable under 10 min electron beam irradiation with beam currents of 400 nA, 600 nA, and 800 nA at 20 kV. Therefore, the high beam currents tested above do not significantly affect F and Cl analysis in olivine. Moreover, the X-ray intensities of F, Cl, and the absorbed beam currents in the Kakanui hornblende standard remain steady (Additional file 1: Fig. S4). According to the detection limit equation, a higher beam current leads to a lower detection limit (e.g., Jercinovic and Williams 2005; Jercinovic et al. 2008; Donovan et al. 2011). However, the detection limit decreases slightly when the beam current is higher than 800 nA for trace elements in olivine (Batanova et al. 2015). Therefore, we choose 800 nA as the optimal beam current to lower the F and Cl detection limits in this study.

3.3 Peak overlaps and background interference

For trace F and Cl analysis in olivine, the peak overlap difficulty lies in dealing with the interferences of the F $K\alpha$ peak, whereas the Cl $K\alpha$ peak and backgrounds are not interfered by any characteristic X-rays of major elements in olivine. PC1 analytical crystal could provide a higher count rate for F than normal TAP crystal. However, an overlap of the Fe $L\alpha_1$ peak (shoulder) onto the F $K\alpha$ peak makes analyzing F in olivine difficult when using PC1 crystal. Besides, the second-order Mg $K\alpha$ and $K\beta$ lines may influence the upper background.

Many studies proposed specific methods to solve these problems (Amlı and Griffin 1975; Potts and Tindle 1989; Donovan et al. 1993; Witter and Kuehner 2004;

Table 1 Analytical conditions for major elements and trace F and Cl in olivine by EPMA

Element	Calibration standard	Accelerating voltage (kV)	Beam current standard (nA)	Beam current sample (nA)	Beam size (jμm)	Peak counting time (s)	Background counting time (s)	Analytical crystals	PHA mode (mV)	Bg-(Sinθ * 10 ⁵)	(Sinθ * 10 ⁵)
Si	Rhodonite	20	30	30	5	20	20	TAP	Base line: 1726 Window: 3274	-1500	1500
Ti	Pure TiO ₂	20	30	30	5	20	20	LPET	Integral	-500	500
Al	Pure Al ₂ O ₃	20	30	30	5	20	20	TAP	Base line: 1347 Window: 3464	-800	1000
Fe	Pure Fe ₂ O ₃	20	30	30	5	60	60	LIF	Integral	-1000	1000
Mg	Pure MgO	20	30	30	5	20	20	TAP	Base line: 1004 Window: 3182	-2000	2000
Mn	Rhodonite	20	30	30	5	10	10	LIF	Integral	-800	1000
Ca	Dropside	20	30	30	5	10	10	LPET	Integral	-600	600
Na	Albite	20	10	30	5	6	6	TAP	Integral	-800	800
K	K-feldspar	20	10	30	5	10	10	LPET	Integral	-700	700
F	MgF ₂	20	10	800	5	240	240	PC1	Base line: 2300 Window: 2170	0	1100
Cl	Halite	20	10	800	5	240+240	240+240	2 LPET	Integral	-600	600

Zhang et al. 2016; Flemetakis et al. 2020). Amli and Griffin (1975) introduced a simple X-ray intensity correction method based on empirical correction factors. The interference correction factors from Fe and Mg were first reported by measuring fayalite and magnesium oxide (Potts and Tindle 1989). Donovan et al. (1993) then developed a refined method that used magnetite to calibrate the interference with Fe $L\alpha$ in determining F but ignored Mg. This method could be incorporated into the analytical software, and the following studies further expanded these earlier results. Witter and Kuehner (2004) developed an empirical method to analyze trace F in Fe-bearing samples, which used several Fe-bearing and F-free minerals and glasses to establish a calibration line to correct Fe-F interference. However, this study also neglected the potential Mg $K\beta$ line interference on the measured upper background. Recently, Zhang et al. (2016) utilized an optimized PHA (pulse height analysis) setting in differential mode to minimize the background interference from Mg $K\beta$ ($n=2$). The overlapping first-order Fe $L\alpha$ on the F $K\alpha$ peak was calibrated quantitatively using a few F-free and Fe-bearing silicate glasses and minerals. Their method successfully obtained trace F concentrations in glasses (Flemetakis et al. 2020; Zhang et al. 2022a), with precision and accuracy confirmed by many well-characterized glass standards.

It is worth noting that the calibration lines would be influenced by instrument types, analytical conditions (e.g., beam currents, PHA settings), and sample types (minerals types or glasses) (Zhang et al. 2016). For minerals, Zhang et al. (2016) used anorthite, pyroxene, garnet, and olivine with FeO content variations from ca. 0.4–17 wt% to build the calibration line ($R^2=0.964$ at 180 nA and $R^2=0.989$ at 60 nA), which are suitable for most F-bearing minerals from the Earth. However, olivine in lunar samples shows wide FeO content variations from ca. 21 wt% to ca. 67 wt% (Butler 1972; Schnare et al. 2008; Snape et al. 2014; Zhang et al. 2022a). As olivine shows a large variation of Mg and Fe concentration and does not contain large amounts of Ca, Al, Ti, and Mn, matrix-matched samples would be preferred to build the calibration line. To improve the calibrations of Fe-F interferences in olivine, we collected San Carlos olivine that was commonly used as a blank sample of F during SIMS analysis (Potts et al. 2021), synthetic F-free olivine samples with Fo values ranging from 0 to 70, and a synthetic MgO sample to build the calibration line. Representative compositions of these samples are shown in Additional file 2: Table S1.

Using this empirical correction method, background counts of F were only collected for the upper background position ($+1100, \text{Sin}\theta^*10^5$), and the differential mode was used with an optimized PHA setting (baseline

2300 mV, window 2170 mV) to minimize the interferences from the second-order Mg $K\beta$ line (Additional file 1: Fig. S5). A traditional 2-point linear background fit and the integral mode were used for trace Cl analysis in olivine. The detailed analytical settings, including calibration standards, peak/background counting times, background positions, and analytical crystals, are listed in Table 1. Matrix effects were corrected using the CAMECA software X-PHI method (Merlet 1994). Oxygen was calculated by cation stoichiometry and included in the matrix correction.

4 Results and discussion

4.1 Calibration lines

The calibration curves are depicted in Fig. 2, and the results are presented in Table 2 and Additional file 2: Table S1. Every point in Fig. 2 represents the average value of five measurements. Our analyses show a linear relationship between the “apparent” F signal and FeO contents; thus, the results may be described by the following linear equation: $y=52.625x+472$ with $R^2=0.9931$. The standard deviation of this linear equation is about 130 ppm based on statistical calculation. When the FeO content is ~ 35 wt%, the 2σ uncertainty (95% confidence) on the “apparent” F content is about ± 140 ppm. This calibration line (Fig. 2) was then used to correct our measured F concentrations in the hornblende and the natural olivine samples mentioned above.

4.2 Detection limit, precision, and accuracy of trace F and Cl in olivine

We treat the Kakanui and Arenal hornblende standards as unknown samples to evaluate the detection limit, precision, and accuracy. The analytical results are listed in Additional file 2: Table S2. The detection limits (3σ) were calculated by CAMECA software based on the equation suggested by Ancey et al. (1978). In our developed method, the detection limits (3σ) for F and Cl are 30 ppm and 5 ppm, respectively, which are significantly lower than those in previous studies (Witter and Kuehner 2004; Zhang et al. 2016).

The analytical precision (reproducibility) established by 15 repeated measurements of the hornblende is 30–50 ppm and 10 ppm for F and Cl (2 sd), respectively (Fig. 3). The average errors of each analysis (2 standard deviations) for F and Cl are 20 ppm and 4 ppm, respectively. As there are no reference values for trace F and Cl in hornblende defined by other methods, the accuracy was tested by comparing the analyses of hornblende samples with the EPMA data published by Zhang et al. (2016). As shown in Fig. 4, the average values of the 15 analyses for the trace F and Cl in Kakanui hornblende and Arenal hornblende are consistent with the reference

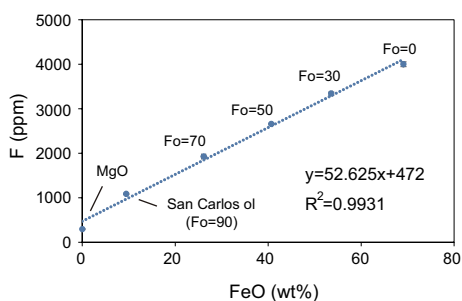


Fig. 2 Calibration line for F. San Carlos olivine, synthetic olivines with Fo ranging from 0 to 70, and MgO were used to build the calibration line

values within error. The average values of F in Kakanui hornblende and Arenal hornblende are 1697 ± 50 ppm and 383 ± 30 ppm (2sd), respectively, which are in good agreement with the reference data (1673 ± 51 ppm for Kakanui hornblende, 361 ± 46 ppm for Arenal hornblende) (Zhang et al. 2016). Fifteen measurements of the Kakanui hornblende and the Arenal hornblende give the Cl average value of 217 ± 10 ppm and 198 ± 10 ppm (2sd), respectively, broadly consistent within error with the literature data (Wolff 2014; Zhang et al. 2016). All data plot well along the 1:1 correspondence line within the precision of methods (Fig. 4a and b).

Table 2 Averaged analytical results for San Carlos olivine, synthetic olivine, and MgO by new EPMA method

Sample	Na ₂ O (wt%)	MgO (wt%)	CaO (wt%)	MnO (wt%)	FeO (wt%)	SiO ₂ (wt%)	F (ppm)	Total (wt%)
Synthetic ol (Fo=0)	0.12 ± 0.10	bdl	bdl	bdl	69.11 ± 0.18	29.70 ± 0.66	4000 ± 108	99.32 ± 0.60
Synthetic ol (Fo=30)	bdl	13.07 ± 0.36	bdl	bdl	53.58 ± 0.50	32.72 ± 0.44	3340 ± 68	99.76 ± 0.70
Synthetic ol (Fo=50)	bdl	23.89 ± 0.50	bdl	0.16 ± 0.06	40.67 ± 0.34	35.17 ± 0.42	2656 ± 30	100.21 ± 0.70
Synthetic ol (Fo=70)	bdl	35.67 ± 0.60	bdl	0.12 ± 0.06	26.14 ± 0.86	37.74 ± 0.70	1927 ± 18	99.87 ± 1.04
San Carlos ol	bdl	49.04 ± 0.38	0.10 ± 0.02	0.16 ± 0.04	9.48 ± 0.26	40.69 ± 0.24	1086 ± 32	99.56 ± 0.66
Synthetic MgO	bdl	99.81 ± 0.32	bdl	bdl	bdl	bdl	295 ± 22	99.84 ± 0.32

Data are given in 2 standard deviations. bdl: below detection limit

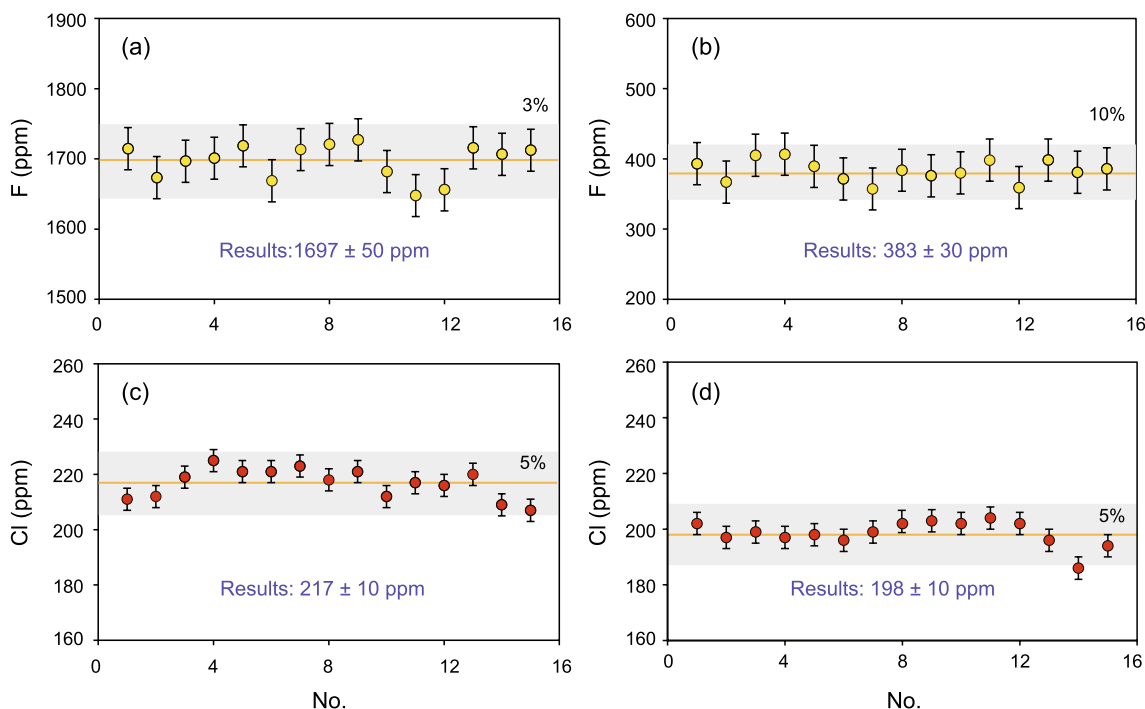


Fig. 3 Fifteen data results on the hornblende standards for trace F and Cl. The shaded portion represents the 3–10% margin of error. The solid line represents the average value. Error bars = 2 standard deviations

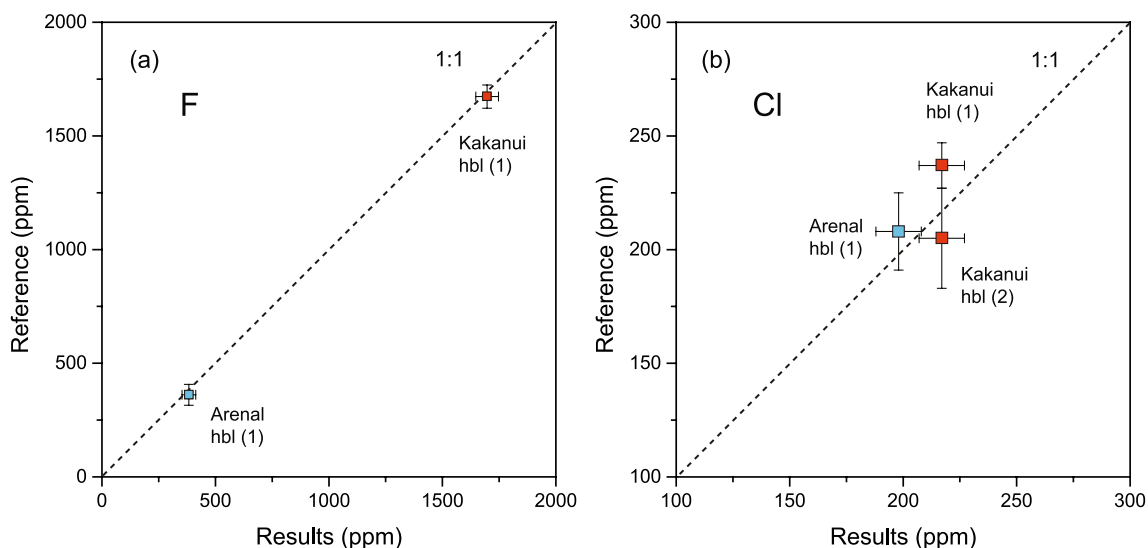


Fig. 4 Comparison of trace F (a) and Cl contents (b) in hornblende standards obtained by optimized EPMA method with reference data. (Error bar = 2 standard deviations). (1) Reference data are from Zhang et al. (2016). (2) Reference data are from Wolff (2014)

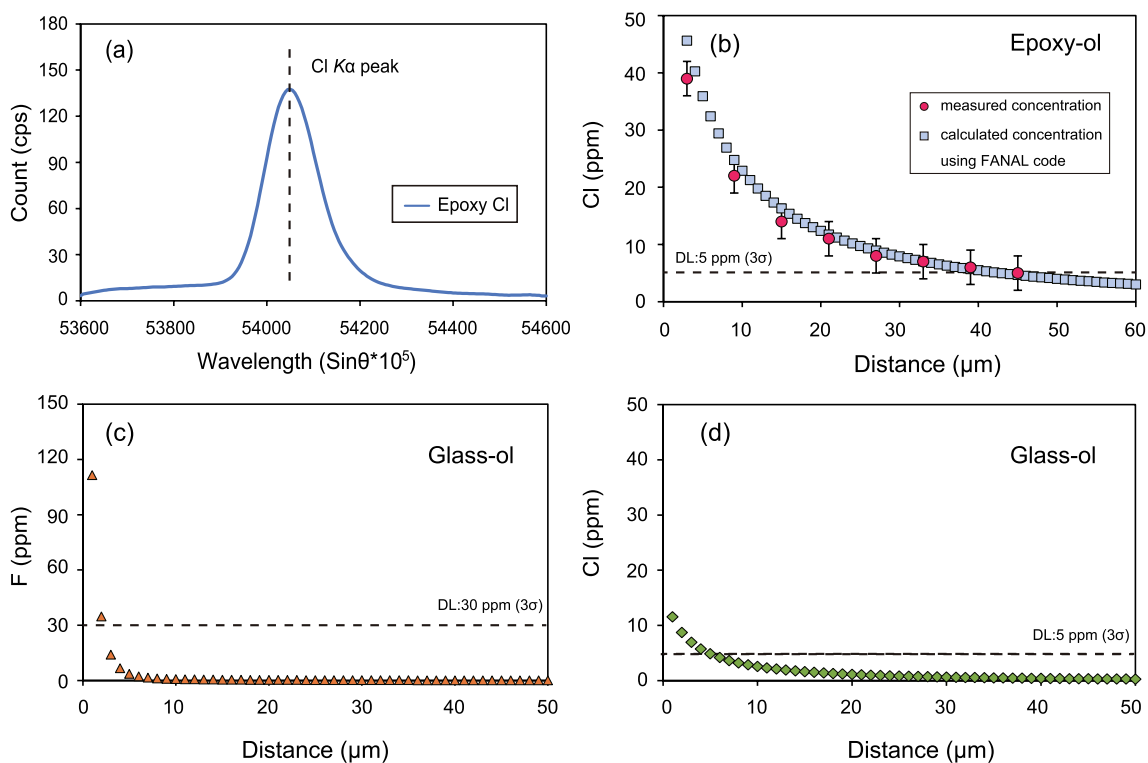


Fig. 5 a Smoothed averaged accumulated spectral scans of epoxy resin at the Cl K α peak acquired with LPET diffraction crystal on CAMECA SXFive microprobe. Accelerating voltage = 15 kV; beam current = 10 nA; beam diameter = 100 μ m; dwell time = 500 ms; step = 5 ($\text{Sin}\theta \cdot 10^5$); and accumulation number = 5. b Secondary fluorescence effects of epoxy resin on trace Cl analysis in olivine using the new method. Error bar = 3 ppm (2 sd). c Secondary fluorescence effects evaluation of F in olivine from the boundary glass using FANAL computer code in CalcZAF/Standard software. d Secondary fluorescence effects evaluation of Cl in olivine from the boundary glass using FANAL computer code in CalcZAF/Standard software

4.3 Secondary fluorescence effects of adjacent phases on trace F and Cl analysis in olivine

The accuracy of trace elemental analysis by EPMA would be affected by secondary fluorescence effects from adjacent phases, which are generated by characteristic and bremsstrahlung X-ray emissions during electron–specimen interactions. The primary X-rays penetrate the specimen in all directions and can further ionize atoms at distances over several tens to hundreds of microns (Fournelle 2005; Llovet et al. 2012; Borisova et al. 2018). Mineral or glass grains are often embedded in epoxy resin for analysis, which is easier to be made and polished than metal mounts. The main epoxy resin component is epichlorohydrin polymer which contains chlorine (Fig. 5a). Different commercially available epoxy resins contain various amounts of Cl as Edinburgh SIMS lab reported (2021). According to the energy-dispersive X-ray spectrums of the resins in their study, the highest Cl intensities in epoxy resin could be ten times to the lowest under the same analytical condition. When the analyzed point is located at the edge of the sample and is close to the epoxy resin, trace Cl analysis in olivine will be affected by the secondary fluorescence effect of epichlorohydrin polymer, leading to lower accuracy and large errors. In addition, olivine is an early crystallizing phase in most mafic magmas and could be hosted by matrix glass (e.g., Davis et al. 2003; Scott et al. 2015; Moussallam et al. 2019). The F and Cl in matrix glass could compromise the accuracy of trace F and Cl analysis in olivine using EPMA. Therefore, these two important cases of secondary fluorescence effects are considered here.

Firstly, San Carlos olivine samples were mounted both in epoxy resin (made in SIMS lab at IGGCAS and numbered as epoxy 128) and tin metal (Additional file 1: Fig. S6) to establish the secondary fluorescence effect of epoxy resin. Profiles were conducted from the grain boundary to the grain core with a length of ~60 μm . As shown in

Fig. 5b, the epoxy resin would bring about ~40 ppm Cl when the analytical position is 3 microns to the olivine boundary. However, Cl concentration of the olivine grain mounted in tin metal could not be detected at the same position (Additional file 2: Table S3). The secondary fluorescence effect of Cl by epoxy resin can be neglected when choosing the analytical position of >40 μm to the boundary (Fig. 5b). As different epoxy resins contain various contents of Cl, the choice of epoxy resin used will significantly impact the magnitude of the secondary fluorescence observed. The safe analytical position will be changed for various kinds of epoxy resin. It also should be noted that this is not the case for glass or other minerals, which need similar tests to ensure safe analytical positions.

Secondary fluorescence effects can be corrected using additional software with a known composition of epoxy resin and an appropriate geometry model, such as the FANAL computer code in CalcZAF/Standard software (Llovet et al. 2012; Borisova et al. 2018). Compositions of epoxy resin were obtained using an element analyzer (Elementar vario EL cube) and ion chromatograph (ICS1100) at East China University of Science and Technology. The epoxy 128 contains 5243 ppm Cl (Additional file 2: Table S4). Given that FANAL considers an ideal material couple consisting of two semi-infinite media separated by a plane boundary perpendicular to the sample surface, which is a similar geometry mode to our profile test (Additional file 1: Fig. S6), a simple evaluation is proposed here. As shown in Fig. 5b, the concentration of Cl obtained from secondary fluorescence effects using software is consistent with the measured results.

A simple simulation using FANAL code was given here to show the secondary fluorescence effects of boundary glass on trace F and Cl analysis in olivine. Matrix glass and olivine phenocrysts compositions were taken from Moussallam et al. (2019). The average F and Cl contents

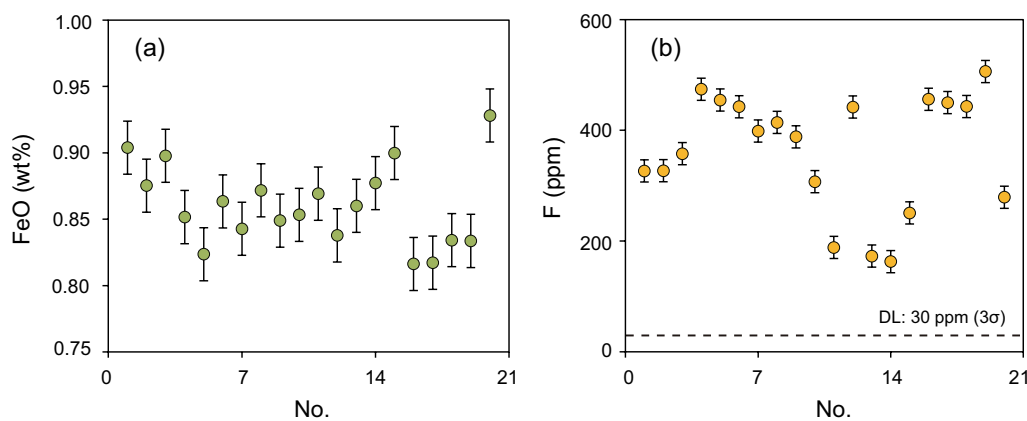


Fig. 6 FeO (a) and F concentrations (b) of natural olivine (OL-1). FeO: error bar = 0.02 wt% (2 sd); F: error bar = 3 ppm (2 sd)

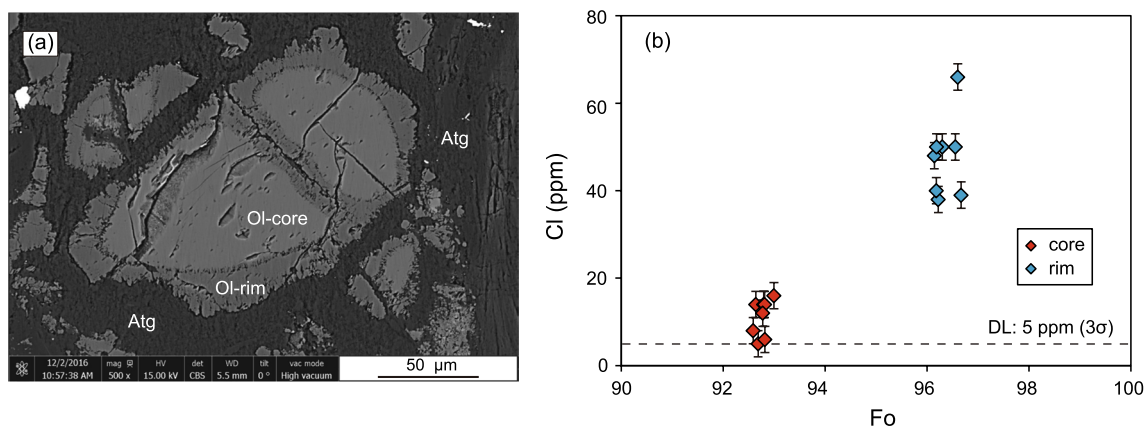


Fig. 7 **a** Backscattered electron image of relict olivine (Ol-2) in Ol-Atg serpentinite. **b** Fo versus Cl plots of Ol-2

of the matrix glass are 620 ppm and 3620 ppm, respectively. As shown in Fig. 5c and d, the adjacent glass would only bring about 4 ppm F and 5 ppm Cl when the analytical position is 5 microns to the olivine boundary. Therefore, the secondary fluorescence effects in this case can be neglected.

5 Application to natural olivine

A promising application of our EPMA method lies in analyzing the F and Cl contents of natural olivine. Here, we apply our new method to the natural olivine samples (Ol-1 and Ol-2).

Random analyses were conducted for several grains of Ol-1 sample, which were mounted in epoxy resin. To avoid the secondary fluorescence effects from Cl in epoxy resin, analytical positions were at least 50 μm away from the boundaries. Representative results are listed in Additional file 2: Table S5. The investigated olivine is typical forsterite with Fo values of ~ 99 . FeO content shows little variations from 0.82 to 0.93 wt% (Additional file 2: Table S5, Fig. 6a). Such little variations of FeO content could lead to similar Fe-F interferences, such as 515 ppm for the lowest FeO content (0.82 wt%) and 521 ppm for the highest FeO content (0.93 wt%). The acquired F contents of olivine samples fluctuated remarkably, with concentrations ranging from 681 to 1022 ppm. After calculating the Fe-F interferences using the equation shown in Fig. 2, the real F concentrations of the investigated olivine are 163–506 ppm (Fig. 6b), which is much higher than the detection limit of 30 ppm. The results indicate that the investigated olivine sample Ol-1 has heterogeneous F concentrations, even with homogeneous Fo values.

Further analyses were performed for natural olivine sample Ol-2 from a forearc Ol-Atg serpentinite in a thin section (Fig. 7a). In this case, secondary fluorescence effects from epoxy resin do not exist. Moreover,

the surrounding antigorite contains only several hundred ppm of Cl (Additional file 2: Table S6), suggesting that the secondary fluorescence effect of Cl caused by the adjacent antigorite might be very limited. We used the computer code FANAL of the CalcZAF/Standard software to test this idea. At a distance of 1 μm to the olivine boundary, the concentration of Cl obtained from secondary fluorescence effects is below 1 ppm (Additional file 1: Fig. S7). Therefore, the secondary fluorescence effects of antigorite on Cl analysis in olivine can be neglected. Ol-2 exhibits bright cores and dark rims (Fig. 7a). The bright olivine cores are characterized by high Fo values (92.6–93.0) and low Cl contents (6–16 ppm), whereas the dark rims are relatively Mg- (Fo: 96.1–96.7) and Cl-rich (38–66 ppm) (Additional file 2: Table S7, Fig. 7b). As the dark rims were produced by the dehydration of antigorite (Chen et al. 2018), their high Cl contents indicate that the newly formed olivine would inherit some Cl-rich signatures of preexisting antigorite.

In summary, our new method can apply well to natural olivine samples and determine trace F and Cl heterogeneity within micron scales.

6 Conclusion

An optimized analytical method for high precision measurement of trace F and Cl in olivine, simultaneously with major elements, was developed using the CAMECA SXFive EPMA. The optimal analytical conditions used for trace F and Cl analysis in olivine were as follows: accelerating voltage of 20 kV, beam current of 800 nA, 5 μm beam diameter, using PC1 analytical crystal for trace F analysis, and several F-free olivine samples with various Fo values and synthetic MgO crystal to calculate Fe-F interferences, and utilizing large-area analytical crystals and aggregate counting strategy for trace Cl analysis. Secondary fluorescence effects on trace Cl analysis in olivine

by epoxy resin can be neglected when choosing the analytical position of $>40 \mu\text{m}$ to the boundary. Replicate analyses on hornblende standards using the proposed optimized method show good agreement with the reference data. Detection limits (3σ) of F and Cl could be lowered to 30 ppm and 5 ppm, respectively. This optimized method can fully exert the advantages of the nondestructive nature, high spatial resolution, high precision and accuracy, and low detection limit of EPMA. Our method would open a new perspective on the study of geochemical processes involving F- and Cl-bearing olivine.

Abbreviations

SIMS	Secondary ion mass spectrometry
EPMA	Electron probe microanalysis
Ol	Olivine
Atg	Antigorite

Supplementary Information

The online version contains supplementary material available at <https://doi.org/10.1186/s40645-023-00561-3>.

Additional file 1. Fig. S1. Backscattered electron images of synthetic olivine samples. **Fig. S2.** Backscattered electron images of natural olivine samples. (a) and (b): Ol-1; (c) and (d): Ol-2. **Fig. S3.** Count rates for F (a) and absorbed beam current (b) for natural Ol-1 olivine sample over 600 s measurements with various beam currents of 400, 600, and 800 nA. The 2 standard deviations of count rates for F for Ol-1 at 400, 600, and 800 nA were 42, 60 and 62 cps, respectively. Count rates for Cl (c) and absorbed beam current (d) for natural Ol-2 olivine sample over 600 s measurements with various beam currents of 400, 600, and 800 nA were 26, 30 and 32 cps, respectively. (Accelerating voltage: 20 kV, beam diameter: 5 μm). **Fig. S4.** Count rates for F (a), Cl (b), and absorbed beam current (c) for Kakanui hornblende standard over 600 s measurements with various beam currents of 400, 600, and 800 nA (Accelerating voltage: 20 kV, beam diameter: 5 μm). The 2 standard deviations of count rates for F for Kakanui hornblende at 400, 600, and 800 nA were 52, 60 and 82 cps, respectively. The 2 standard deviations of count rates for Cl for Kakanui hornblende at 400, 600, and 800 nA were 37, 45 and 51 cps, respectively. **Fig. S5.** (a) Smoothed averaged accumulated spectral scans of Kakanui hornblende at the F K α peak using integral and differential mode on CAMECA SXFive microprobe. The second-order Mg K β line was minimized using the optimized differential mode compared to the integral mode. Accelerating voltage = 20 kV; beam current = 150 nA; beam diameter = 10 μm ; dwell time = 500 ms; step = 10 ($\text{Sin}\theta^*10^5$); accumulation number = 5; differential mode: base line = 2300 mV, window = 2170 mV, PC1 analyzing crystal. **Fig. S6.** Backscattered electron images of San Carlos olivine samples mounted in epoxy resin (a) and tin metal (b). **Fig. S7.** Secondary fluorescence effects evaluation of Cl in natural olivine (Ol-2) from the boundary antigorite using FANAL computer code in CalcZAF/Standard software

Additional file 2. Table S1. Analytical results for trace F and Cl in San Carlos olivine, synthetic olivine and MgO by new EPMA method. **Table S2.** Analytical results for trace F and Cl in hornblende standards by new EPMA method. **Table S3.** Analytical results of secondary fluorescence effects of San Carlos olivines mounted in epoxy resin and tin metal. **Table S4.** Compositions of (wt%) epoxy-128 used in this study obtained using element analyzer and ion chromatograph. **Table S5.** Analytical results for trace F and Cl in natural olivine (Ol-1) by new EPMA method. **Table S6.** Representative compositions (wt%) of antigorite adjacent to olivine sample (Ol-2). **Table S7.** Representative compositions (wt%) of olivine sample (Ol-2).

Acknowledgements

We thank Prof. John Fournelle for inspiring discussions on the early draft.

Author contributions

YC conceived this study and edited the manuscript. DZ carried out the experimental study, analyzed the data, and wrote the draft manuscript. CQ synthesized the olivine samples. BS helped to edit the manuscript. QM contributed to the method establishment and data interpretation. All authors read and approved the final manuscript.

Funding

This study was financially supported by the National Key R&D Program of China (2018YFA0702601), the Key Research Program of Chinese Academy of Sciences (ZDBS-SSW-JSC007-15), and the Experimental Technology Innovation Fund (11990890) and the Key Research Program (IGGCAS-202101) of the Institute of Geology and Geophysics, Chinese Academy of Sciences.

Availability data and materials

All data generated or analyzed during this study are included in this article and its additional files.

Declarations

Competing interests

The authors declare that they have no competing interests.

Received: 11 January 2023 Accepted: 5 June 2023

Published online: 12 June 2023

References

- Almasi GS, Blair J, Ogilvie RE, Schwartz RJ (1965) A heat-flow problem in electron-beam microprobe analysis. *J Appl Phys* 36(6):1848–1854
- Amlı R, Griffin WL (1975) Microprobe analysis of REE minerals using empirical correction factors. *Am Miner* 60(7–8):599–606
- Ancey M, Bastenaire F, Tixier R (1978) Applications of statistical methods in microanalysis. In: Maurice F (ed.), *Proc. Summer School St. Martin-d'Herres*. Les Editions de Physique, Orsay, France, pp 319–343
- Antignano A, Manning CE (2008) Fluorapatite solubility in H₂O and H₂O–NaCl at 700 to 900 °C and 0.7 to 2.0 GPa. *Chem Geol* 251:112–119
- Bartels A, Vetere F, Holtz F, Behrens H, Linnen RL (2011) Viscosity of flux-rich pegmatitic melts. *Contrib Mineral Petrol* 162:51–60
- Batanova VG, Sobolev AV, Kuzmin DV (2015) Trace element analysis of olivine: High precision analytical method for JEOL JXA-8230 electron probe microanalyser. *Chem Geol* 419:149–157
- Bernini D, Wiedenbeck M, Dolejš D, Keppler H (2013) Partitioning of halogens between mantle minerals and aqueous fluids: implications for the fluid flow regime in subduction zones. *Contrib Miner Petrol* 165:117–128
- Beyer C, Klemme S, Wiedenbeck M, Stracke A, Vollmer C (2012) Fluorine in nominally fluorine-free mantle minerals: Experimental partitioning of F between olivine, orthopyroxene and silicate melts with implications for magmatic processes. *Earth Planet Sci Lett* 337–338:1–9
- Borisova AY, Zagrtednov NR, Toplis MJ, Donovan JJ, Llovet X, Asimow PD, de Parseval P, Gouy S (2018) Secondary fluorescence effects in microbeam analysis and their impacts on geospeedometry and geothermometry. *Chem Geol* 490:22–29
- Borom MP, Hanneman RE (1967) Local compositional changes in alkali silicate glasses during electron microprobe analysis. *J Appl Phys* 38(5):2406–2407
- Botcharnikov RE, Linnen RL, Holtz F (2010) Solubility of Au in Cl- and S-bearing hydrous silicate melts. *Geochim Cosmochim Acta* 74:2396–2411
- Bucher K, Stober I (2010) Fluids in the upper continental crust. *Geofluids* 10:241–253
- Butler P (1972) Compositional characteristics of olivines from Apollo 12 samples. *Geochim Cosmochim Acta* 36:773–785
- Chen M (2005) The formation conditions of ringwoodite in meteorites: clues to finding terrestrial ringwoodite. *Earth Sci Front* 12:23–27

- Chen Y, Huang F, Shi GH, Wu FY, Chen X, Jin QZ, Su B, Guo S, Sein K, Nyunt TT (2018) Magnesium isotope composition of subduction zone fluids as constrained by jadeitites from Myanmar. *J Geophys Res Solid Earth* 123:7566–7585
- Clarke E, De Hoog J, Kirstein L, Harvey J, Debret B (2020) Metamorphic olivine records external fluid infiltration during serpentinite dehydration. *Geochem Persp Lett* 16:25–29
- Crépeiron C, Blanchard M, Bureau H, Sanloup C, Withers AC, Khodja H, Surlblé S, Raepsaet C, Béneut K, Leroy C, Giura P, Balan E (2014) Clumped fluoride-hydroxyl defects in forsterite: implications for the upper-mantle. *Earth Planet Sci Lett* 390:287–295
- Dalou C, Koga KT, Shimizu N, Boulon J, Devidal JL (2012) Experimental determination of F and Cl partitioning between lherzolite and basaltic melt. *Contrib Miner Petrol* 163:591–609
- Davis MG, Garcia MO, Wallace P (2003) Volatiles in glasses from Mauna Loa Volcano, Hawaii: implications for magma degassing and contamination, and growth of Hawaiian volcanoes. *Contrib Miner Petrol* 144:570–591
- Debret B, Koga KT, Nicollet C, Andreani M, Schwartz S (2014) F, Cl and S input via serpentinite in subduction zones: implications for the nature of the fluid released at depth. *Terra Nova* 26:96–101
- Donovan JJ, Snyder DA, Rivers ML (1993) An improved interference correction for trace element analysis. *Microbeam Anal* 2:23–28
- Donovan JJ, Lowers HA, Rusk BG (2011) Improved electron probe microanalysis of trace elements in quartz. *Am Miner* 96:274–282
- Edinburgh SIMS lab (2021) <https://www.ed.ac.uk/geosciences/about/facilities/all/ionprobe/instrument-capabilities-and-sample-requirements/specimen-requirements/epoxy-resins/results/compositions>. Accessed 20 Mar 2023
- Filiberto J, Reiman AH (2009) The effect of chlorine on the liquidus of basalt: first results and implications for basalt genesis on Mars and Earth. *Chem Geol* 263:60–68
- Flemetakis S, Berndt J, Klemme S, Genske F, Cadoux A, Louvel M, Rohrbach A (2020) An improved electron microprobe method for the analysis of halogens in natural silicate glasses. *Microsc Microanal* 26:857–866
- Fournelle JH, Kim S, Perepezko JH (2005) Monte Carlo simulation of Nb K α secondary fluorescence in EPMA: comparison of PENELOPE simulations with experimental results. *Surf Interface Anal* 37:1012–1016
- Grützner T, Klemme S, Rohrbach A, Gervasoni F, Berndt J (2018) The effect of fluorine on the stability of wadsleyite: implications for the nature and depths of the transition zone in the Earth's mantle. *Earth Planet Sci Lett* 482:236–244
- Hermann J, Fitz Gerald JD, Malaspina N, Berry AJ, Scambelluri M (2007) OH-bearing planar defects in olivine produced by the breakdown of Ti-rich humite minerals from Dabie Shan (China). *Contrib Miner Petrol* 153(4):417–428
- Hervig R, Bell D (2005) Fluorine and hydrogen in mantle megacrysts. *Am Geophys Union Fall Meet* 41:1426
- Jercinovic MJ, Williams ML (2005) Analytical perils (and progress) in electron microprobe trace element analysis applied to geochronology: Background acquisition, interferences, and beam irradiation effects. *Am Miner* 90:526–546
- Jercinovic MJ, Williams ML, Lane ED (2008) In-situ trace element analysis of monazite and other fine-grained accessory minerals by EPMA. *Chem Geol* 254:197–215
- Joachim B, Stechern A, Ludwig T, Konzett J, Pawley A, Ruzié-Hamilton L, Clay PL, Burgess R, Ballentine CJ (2017) Effect of water on the fluorine and chlorine partitioning behavior between olivine and silicate melt. *Contrib Miner Petrol* 172:15
- Johann HH (1931) Die Erzeugung lichtstarker Röntgenspektren mit Hilfe von Konkavkristallen. *Z Phys* 69:185–206
- Johansson T (1933) Über ein neuartiges, genau fokussierendes Röntgenspektrometer. *Z Phys* 82:507–528
- Kendrick MA, Honda M, Vanko DA (2015) Halogens and noble gases in Mathematician Ridge meta-gabbros, NE Pacific: implications for oceanic hydrothermal root zones and global volatile cycles. *Contrib Miner Petrol* 170:1–20
- Keppler H (1993) Influence of fluorine on the enrichment of high field strength trace elements in granitic rocks. *Contrib Miner Petrol* 114:479–488
- Klemme S, Stalder R (2018) Halogens in the Earth's Mantle: what we know and what we don't. In: Harlov DE, Aranovich L (eds) *The Role of halogens in terrestrial and extraterrestrial geochemical processes: surface, crust, and mantle*. Springer International Publishing, Cham, pp 847–869
- Kusebauch C, John T, Barnes JD, Klügel A, Austrheim HO (2015) Halogen element and stable chlorine isotope fractionation caused by fluid–rock interaction (Bamble Sector, SE Norway). *J Petrol* 56:299–324
- Li X, Liu Y, Wang R, Yoshino T, Xu J, Zhang D, Grützner T, Zhang J, Wu X (2022) Thermal equation of state of F-bearing superhydrous phase B (Mg₁₀Si₃O₁₄(OH, F)₄): Implications for the transportation of fluorine and water into the lower mantle. *Phys Earth Planet Inter* 323:106824
- Llovet X, Pinard PT, Donovan JJ, Salvat F (2012) Secondary fluorescence in electron probe microanalysis of material couples. *J Phys D Appl Phys* 45:225301
- McCubbin FM, Jolliff BL, Nekvasil H, Carpenter PK, Zeigler RA, Steele A, Elardo SM, Lindsley DH (2011) Fluorine and chlorine abundances in lunar apatite: implications for heterogeneous distributions of magmatic volatiles in the lunar interior. *Geochim Cosmochim Acta* 75:5073–5093
- Merlet C (1994) An accurate computer correction program for quantitative electron probe microanalysis. *Microchim Acta* 114(115):363–376
- Morgan GB, London D (1996) Optimizing the electron microprobe analysis of hydrous alkali aluminosilicate glasses. *Am Miner* 81(9–10):1176–1185
- Morgan GB, London D (2005) Effect of current density on the electron microprobe analysis of alkali aluminosilicate glasses. *Am Miner* 90(7):1131–1138
- Mosenfelder JL, Rossman GR (2013a) Analysis of hydrogen and fluorine in pyroxenes: I. Orthopyroxene. *Am Miner* 98:1026–1041
- Mosenfelder JL, Rossman GR (2013b) Analysis of hydrogen and fluorine in pyroxenes: II. Clinopyroxene. *Am Miner* 98:1042–1054
- Mosenfelder JL, Le Voyer M, Rossman GR, Guan Y, Bell DR, Asimow PD, Eiler JM (2011) Analysis of hydrogen in olivine by SIMS: Evaluation of standards and protocol. *Am Miner* 96:1725–1741
- Moussallam Y, Rose-Koga EF, Koga KT, Médard E, Bani P, Devidal JL, Tari D (2019) Fast ascent rate during the 2017–2018 Plinian eruption of Ambae (Aoba) volcano: a petrological investigation. *Contrib Miner Petrol* 174:90–113
- Potts PJ, Tindle AG (1989) Analytical characteristics of a multilayer dispersion element (2d = 60 Å) in the determination of fluorine in minerals by electron microprobe. *Miner Mag* 53:357–362
- Potts NJ, Bromiley GD, Brooker RA (2021) An experimental investigation of F, Cl and H₂O mineral–melt partitioning in a reduced, model lunar system. *Geochim Cosmochim Acta* 294:232–254
- Roberge M, Bureau H, Bolfan-Casanova N, Frost DJ, Raepsaet C, Surlblé S, Khodja H, Auzende A-L, Fiquet G (2015) Is the transition zone a deep reservoir for fluorine? *Earth Planet Sci Lett* 429:25–32
- Roberge M, Bureau H, Bolfan-Casanova N, Raepsaet C, Surlblé S, Khodja H, Auzende A-L, Cordier P, Fiquet G (2017) Chlorine in wadsleyite and ringwoodite: an experimental study. *Earth Planet Sci Lett* 467:99–107
- Scambelluri M, Fiebig J, Malaspina N, Müntener O, Pettker T (2004) Serpentinite subduction: implications for fluid processes and trace-element recycling. *Int Geol Rev* 46:595–613
- Schnare DW, Day JM, Norman MD, Liu Y, Taylor LA (2008) A laser-ablation ICP-MS study of Apollo 15 low-titanium olivine-normative and quartz-normative mare basalts. *Geochim Cosmochim Acta* 72:2556–2572
- Scott JAJ, Humphreys MCS, Mather TA, Pyle DM, Stock MJ (2015) Insights into the behaviour of S, F, and Cl at Santiaguito Volcano, Guatemala, from apatite and glass. *Lithos* 232:375–394
- Snape JF, Joy KH, Crawford IA, Alexander L (2014) Basaltic diversity at the Apollo 12 landing site: inferences from petrologic examinations of the soil sample 12003. *Meteorit Planet Sci* 49:842–871
- Stormer JC, Pierson ML, Tacker RC (1993) Variation of F and Cl X-ray intensity due to anisotropic diffusion in apatite during electron microprobe analysis. *Am Miner* 78:641–648
- Su B, Chen Y, Mao Q, Zhang D, Jia L-H, Guo S (2019) Minor elements in olivine inspect the petrogenesis of orogenic peridotites. *Lithos* 344–345:207–216
- Tian HC, Wang H, Chen Y, Yang W, Zhou Q, Zhang C, Lin HL, Huang C, Wu ST, Jia LH, Xu L, Zhang D, Li XG, Chang R, Yang YH, Xie LW, Zhang DP, Zhang GL, Yang SH, Wu FY (2021) Non-KREEP origin for Chang'E-5 basalts in the Procellarum KREEP Terrane. *Nature* 600:59–63
- Vanko DA (1986) High-chlorine amphiboles from oceanic rocks: product of highly-saline hydrothermal fluids? *Am Miner* 71:51–59
- Whitney DL, Evans BW (2010) Abbreviations for names of rock-forming minerals. *Am Miner* 95:185–187

- Wirth R, Dobrzhinetskaya LF, Green HW (2001) Electron microscope study of the reaction olivine +H₂O +TiO₂→titanian clinohumite +titanian chondrodite synthesized at 8GPa, 1300K. *Am Miner* 86:601–610
- Witter JB, Kuehner SM (2004) A simple empirical method for high-quality electron microprobe analysis of fluorine at trace levels in Fe-bearing minerals and glasses. *Am Miner* 89:57–63
- Wolff PE (2014) Hydrothermal circulation from very high to low temperatures in the lower oceanic crust: evidence from layered gabbros from the Oman ophiolite and from partial melting experiments on oceanic gabbros. PhD, University of Hannover, p 167
- Zhang C, Holtz F, Ma C, Wolff PE, Li X (2012) Tracing the evolution and distribution of F and Cl in plutonic systems from volatile-bearing minerals: a case study from the Liujiawa pluton (Dabie orogen, China). *Contrib Miner Petrol* 164:859–879
- Zhang C, Koepke J, Wang L-X, Wolff PE, Wilke S, Stechern A, Almeev R, Holtz F (2016) A practical method for accurate measurement of trace level fluorine in Mg- and Fe-bearing minerals and glasses using electron probe microanalysis. *Geostand Geoanal Res* 40:351–363
- Zhang D, Su B, Chen Y, Yang W, Mao Q, Jia L-H (2022a) Titanium in olivine reveals low-Ti origin of the Chang'E-5 lunar basalts. *Lithos* 414–415:106639
- Zhang HL, Zeng G, Zhang C, Zhang WL, Chen LH, Yu JH (2022b) Electron probe microanalysis measurement of F-Cl-Nb-P for geological glasses. *Geostand Geoanal Res* 46(4):851–864
- Zhao YH, Zimmerman ME, Kohlstedt DL (2009) Effect of iron content on the creep behavior of olivine: 1. anhydrous conditions. *Earth Planet Sci Lett* 287:229–240

Publisher's Note

Springer Nature remains neutral with regard to jurisdictional claims in published maps and institutional affiliations.

Submit your manuscript to a SpringerOpen[®] journal and benefit from:

- Convenient online submission
- Rigorous peer review
- Open access: articles freely available online
- High visibility within the field
- Retaining the copyright to your article

Submit your next manuscript at ► [springeropen.com](https://www.springeropen.com)
